Response prediction to a multitargeted kinase inhibitor in cancer cell lines and xenograft tumors using high-content tyrosine peptide arrays with a kinetic readout

Matthias Versele,[1] Willem Talloen,[2] Cindy Rockx,[1] Tamara Geerts,[1] Boud Janssen,[1] Tom Lavrijssen,[1] Peter King,[1] Hinrich W.H. Göhlmann,[3] Martin Page,[1] and Tim Perera[1]

[1]Ortho Biotech Oncology Research and Development, [2]Biometrics and Clinical Informatics, and [3]Functional Genomics, Johnson & Johnson Pharmaceutical Research and Development, Beerse, Belgium

Abstract

Multitargeted kinase inhibitors have shown clinical efficacy in a range of cancer types. However, two major problems associated with these drugs are the low fraction of patients for which these treatments provide initial clinical benefit and the occurrence of resistance during prolonged therapy. Several types of predictive biomarkers have been suggested, such as expression level and phosphorylation status of the major targeted kinase(s), mutational status of the kinases involved and of key components of the downstream signaling cascades, and gene expression signatures. In this work, we describe the development of a response prediction platform that does not require prior knowledge of the relevant kinases targeted by the inhibitor; instead, a phosphotyrosine peptide profile using peptide arrays with a kinetic readout is derived in lysates in the presence and absence of a kinase inhibitor. We show in a range of cell lines and in xenograft tumors that this approach allows for the stratification of responders and nonresponders to a multitargeted kinase inhibitor. [Mol Cancer Ther 2009;8(7):1846–55]

Introduction

Many members of the protein tyrosine kinase family have been identified as proto-oncogenes over the last 25 years and inhibition of tyrosine kinase activity has become an important approach to treat cancer. Imatinib (Gleevec/Glivec) is an effective drug to treat patients with chronic myeloid leukemia (1); imatinib inhibits the constitutive tyrosine kinase activity of BCR-ABL. Imatinib is also effective as a treatment for gastrointestinal tumors (2). The underlying mechanism is that tumorigenesis of gastrointestinal tumors often depends on overactivation of the receptor tyrosine kinases (RTK) cKIT or platelet-derived growth factor receptor α (PDGFRα), both of which are also inhibited by imatinib (3). However, a significant problem associated with imatinib treatment is the occurrence of resistance on prolonged treatment, both in chronic myeloid leukemia and in gastrointestinal tumor (4, 5). Two other approved molecules, erlotinib (Tarceva) and gefitinib (Iressa), are tyrosine kinase inhibitors primarily targeting the epidermal growth factor receptor (EGFR). The clinical efficacy of erlotinib and gefitinib is less impressive than imatinib: the response rate of gefitinib in an unselected non–small cell lung cancer (NSCLC) patient population is between 10% and 20% (6). In addition, acquired resistance occurs frequently and rapidly during treatment with EGFR inhibitors. Hence, the early detection of emerging resistance during treatment, and the stratification of drug-naive patients that are likely to respond to a kinase inhibitor from those that are not, could prevent patients being treated with ineffective agents (and provide the opportunity to timely undergo alternative treatments) and will increase the chances of drug approval in a limited but well-defined patient population. Additionally, during the preclinical development of a drug, these stratification tools can be used to probe for indications with a particularly high fraction of likely responders.

Several examples of such prediction tools have been reported. Activating mutations in EGFR correlate with exquisite sensitivity to gefitinib and erlotinib, both *in vitro* and in the clinic (7–9), although a considerable group of patients lacking mutations in EGFR still benefit from gefitinib and, especially, erlotinib therapy (9, 10). Conversely, secondary mutations in EGFR have been associated with acquired resistance to gefitinib and erlotinib (11, 12), and likewise, mutations in the kinase domains of ABL, cKIT, and PDGFRα have been associated with resistance to imatinib (4, 5). In addition, mutations in key downstream proteins in the RTK signaling cascades that allow for RTK-independent signaling, such as mutationally activated K-RAS and inactivated or deleted PTEN (the PI-3,4,5-P_3 phosphatase that antagonizes phosphatidylinositol 3-kinase), inversely correlate with response to RTK inhibitors in some instances (13, 14). With the advent of genome-wide profiling technology, and instigated by the realization that many kinase inhibitors have multiple targets and that the relevant targets critical for effectiveness of an agent are not

Received 10/31/08; revised 3/24/09; accepted 5/5/09; published OnlineFirst 7/7/09.

The costs of publication of this article were defrayed in part by the payment of page charges. This article must therefore be hereby marked *advertisement* in accordance with 18 U.S.C. Section 1734 solely to indicate this fact.

Requests for reprints: Matthias Versele, Ortho Biotech Oncology Research and Development, Janssen Pharmaceutica, Turnhoutseweg 30, B-2340 Beerse, Belgium. Phone: 32-14603965; Fax: 32-14605403. E-mail: mversele@its.jnj.com

doi:10.1158/1535-7163.MCT-08-1029

always clear (see for example ref. 15), unbiased methods to stratify responders and nonresponders have been suggested. The most widespread methodology makes use of microarray gene expression signatures. In that case, the whole-genome expression profile of several responders is compared with that of nonresponders (before treatment), and genes that are differentially expressed between the two groups can be used to predict the likelihood of unknown cases (see refs. 16–18 for some recent examples). A drawback of this method is that it is not directly related to the mechanism of action of kinase inhibitors and hence relies on indirect parameters to assess responsiveness of a sample. Moreover, this method (and most other response-prediction methods) is based on parameters measured in the untreated sample only. As a consequence, these methods are very sensitive to tumor heterogeneity and sample quality.

Here, we have developed a platform to measure the inhibition of tyrosine kinase activity by small molecules in lysates, prepared from cell lines or tumor samples, using high-content tyrosine peptide arrays. Importantly, this technology directly measures the relevant mechanism of action of a kinase inhibitor and the parameters that correlate with response status are relative values (i.e., the ratio of kinase activity in the lysate in the absence of compound over the activity in the presence of compound). We show for a multitargeted kinase inhibitor, MTKI, that responder cell lines can be discriminated from nonresponder cell lines based on a specific phosphopeptide inhibition profile. The kinases that phosphorylate these "signature peptides" are closely linked to the mechanism of action of the inhibitor (EGFR, Her2, and Src). In addition, we show that also in xenograft tumor lysates, inhibition of the phosphorylation of a specific, partially overlapping, set of peptides by MTKI discriminates responders from nonresponders, indicating that this technology should be applicable to patient stratification.

Materials and Methods

PAMCHIP Procedure

Crude cell lysates, filtered through 0.2-μm filter, were diluted to 1 mg/mL in a total volume of 200 μL, with M-PER buffer containing phosphatase and protease inhibitors (all from Thermo Scientific). Total lysate (10 μg) was applied per well on the PAMCHIP96. The lysate was then 1:1 diluted with compound or DMSO diluted to the appropriate concentration in 10 mmol/L Tris (pH 7.5). Meanwhile, a PAMCHIP96 tyrosine peptide chip (Pamgene) was blocked with 2% bovine serum albumin using the standard setting of a PAMSTATION96 (Pamgene). The composition of the kinase buffer was as follows: 1× ABL buffer (New England Biolabs), 0.5 mg/mL bovine serum albumin (from 10 mg/mL New England Biolabs stock), 100 μmol/L ATP (dissolved and diluted in 1× ABL buffer), and 5 μg/mL PY20-FITC (azide-free preparation; ExAlpha Biologicals). A 2× concentrated kinase buffer was prepared and chilled on ice, and the solution is added 1:1 to the (compound treated) ice-cold lysates and immediately applied to the tyrosine peptide PAMCHIP96. The assay was run on a PAMSTATION96 according to standard procedures: after loading of the plate, the assay mix was pumped once onto the wells, a first exposure was read, and then a kinetic reading program (reading every 5 min) was run for 40 min. Lysates were run in four or six technical replicates and were always applied horizontally next to each other to avoid vertical strip effects of the chip.

Data Analysis

The data (spot images) were further quantified and linked to the peptide identities using EVOLVE PAMGRID software. The quantified data were then fitted to a curve using CurveFitHT software using the Vinip2 curve fitting algorithm, applied on the first 30 min of the assay; the initial velocity is derived at the first kinetic time point read. Replicates from visually damaged wells or with interreplicate correlation coefficients lower than 0.95 were removed from the analysis. All subsequent data analyses were done on initial velocities (V_{ini}) using the software packages Omniviz and R. Standard hierarchical clustering was used to cluster cell lines according to peptide phosphorylation inhibition. All subsequent statistical analysis are described in Supplementary Materials and Methods.

Cell culture methods and reagents, all standard biochemical analysis, and the xenograft tumor studies are in detail described in Supplementary Materials and Methods.

Results

Pamgene Peptide Arrays Allow for the Time-Dependent Detection of Phosphorylation of 144 Tyrosine Peptides in a Single Well of a 96-Well Plate

We have tested the utility of peptides arrayed on a three-dimensional porous matrix, produced and commercialized by Pamgene (see Materials and Methods; ref. 19). The array type we have used in this study contains 144 peptides consisting of 15 amino acids with a tyrosine usually in the middle of the peptide.[4] The 13 COOH-terminal amino acids of each peptide correspond to known or putative phosphorylation sites in a variety of human proteins. Two NH_2-terminal residues are part of a linker sequence and are chemically coupled to the metaloxide solid support. The three-dimensional nature of the matrix results in a high surface area, which allows spotting of high amounts of peptide on a small surface, resulting in high-content peptide arrays: the arrays are the size of 1 well in a 96-well plate and contain 144 spotted peptides (~0.3 pmol peptide per spot) surrounded by a square of spots of reference dye for gridding purposes. The arrays are assembled as a 96-well plate, allowing for many replicate samples to be processed simultaneously under identical conditions. Peptide phosphorylation on these arrays can be measured kinetically using a microfluidic device with an integrated charge-coupled device camera (PAMSTATION96) as explained in Fig. 1. Following the assay, spots are gridded, spot intensities at each time point are quantified (and corrected for local background), and the

[4] See http://www.pamgene.com for a full description.

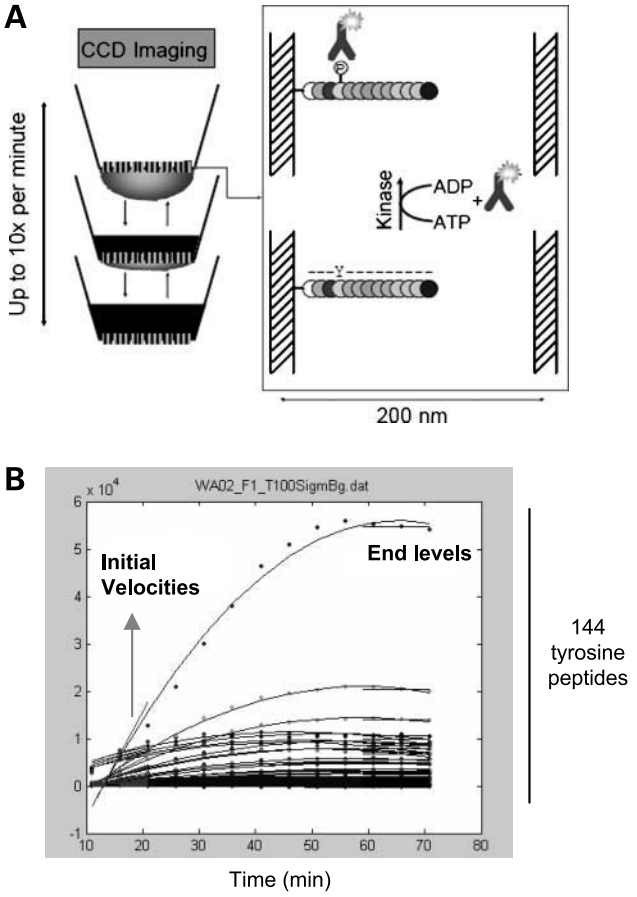

Figure 1. The use of high-content tyrosine peptide arrays with a kinetic readout. **A,** phosphorylation of immobilized tyrosine peptides is detected using PY20-FITC. The assay mix, containing 5 to 10 μg crude lysate or any other source of kinase activity such as recombinant or immunopurified enzymes, ATP, a Mg^{2+}-containing buffer, and the phosphotyrosine antibody PY20 coupled to FITC, is applied to the porous matrix and is continuously pumped up and down through the pores. At 5-min time intervals, the assay mix is pumped underneath a black plate at the bottom of the well, during the time that a charge-coupled device (*CCD*) camera detects from the top of the well the amount of PY20-FITC bound to each peptide on the array. This detection step, which only takes a few milliseconds per well, can be repeated every 5 min throughout the kinase reaction, resulting in the kinetic measurement of the phosphorylation of the peptides. **B,** kinetic analysis of the phosphorylation of 144 peptides (results from 1 array or 1 well of a 96-well plate).

resulting time-resolved curves are fit using appropriate kinetic algorithms. The initial velocity associated with peptide phosphorylation is calculated for each peptide. Further details on this methodology can be found in Materials and Methods and cited references therein.

Src and MET Activity in Cell Lysates Can Be Specifically Measured on the Peptide Arrays

In an initial test to determine whether the arrays are a reliable tool to measure tyrosine kinase activity in crude lysates, we evaluated the ability to detect activity of the cytoplasmic tyrosine kinase, Src, in cell lysates. We transfected HT29 colon carcinoma cells with human Src, expressed by the strong constitutive cytomegalovirus promoter, or with empty vector. Lysates of both transfectants were incubated with either solvent (DMSO) or two different compounds: PP2, a generic Src inhibitor (see ref. 20 for an updated specificity profile), or JNJ-26483327 (hereafter called MTKI; ref. 21). The latter pan-HER tyrosine kinase inhibitor targets, in order of potency, RET, EGFR, Her2, Her4, VEGFR-3, Src, and other Src family kinase members as illustrated in Supplementary Table S2. Both compounds have in common the ability to inhibit Src and Src family members but do not share any other targets (e.g., PP2 is also a PDGFR inhibitor, whereas MTKI completely lacks that activity, and vice versa for EGFR; Supplementary Table S2; refs. 20, 21). Both compounds were used at 5 μmol/L (final concentration on the chip). Lysates were processed in four to six replicates and the initial velocities (hereafter called V_{ini}) of those replicates are shown as a heat map representation in Fig. 2A. HT29 cells already express high levels of Src, but the rate of phosphorylation of some peptides is increased even further on transfection of Src. Conversely, the rate of phosphorylation of a subset of peptides decreases when the lysates are incubated with either of the two Src inhibitors, PP2 or MTKI. Those peptides of which the V_{ini} significantly ($P < 0.05$ in a Student's t test) increased on Src transfection and decreased with both compounds were classified as "Src-selective" peptides and are shown in Fig. 2A. Seven of nine peptides are known Src or Src family kinase substrates showing that phosphorylation of these peptides on the array can correlate to real, cellular phosphorylation sites. To confirm that a similar set of peptides correlates with Src activity in the context of other cell lines, we knocked down Src using small interfering RNA (siRNA) in HCT116 and SKOV-3 cells, both of which express high levels of endogenous Src (see also Supplementary Fig. S1;[5] SKOV-3 data not shown). In spite of the relatively mild conditions of the transient knockdown (25 nmol/L siRNA, 24 hours of incubation), siRNA of Src will likely influence other tyrosine kinase activities in addition to Src itself. Nonetheless, among the peptides of which the phosphorylation rate was significantly ($P < 0.05$) reduced for both siRNAs in both cell lines (highlighted in Supplementary Fig. S1), we found all nine previously identified Src-selective peptides, confirming that this set of peptides is a reliable measure of Src activity in cell lysates.

To examine whether the currently available 144-tyrosine peptide arrays are also useful to detect other tyrosine kinase activities in lysates, particularly RTK activity, we made use of an exquisitely selective inhibitor of the MET RTK, JNJ-38877605 (this inhibitor inhibits MET at 4 nmol/L *in vitro* and does not inhibit any other kinase at <2 μmol/L; ref. 22). Four cell lysates, derived from cell lines expressing high MET levels (the gastric cell lines KatoII, SNU-5, and MKN45 all have MET gene amplifications, and the NSCLC line H441 highly overexpresses the MET protein), were compared with lysates from cells with intermediate (gastric

[5] Supplementary material for this article is available at Molecular Cancer Therapeutics Online (http://mct.aacrjournals.org/).

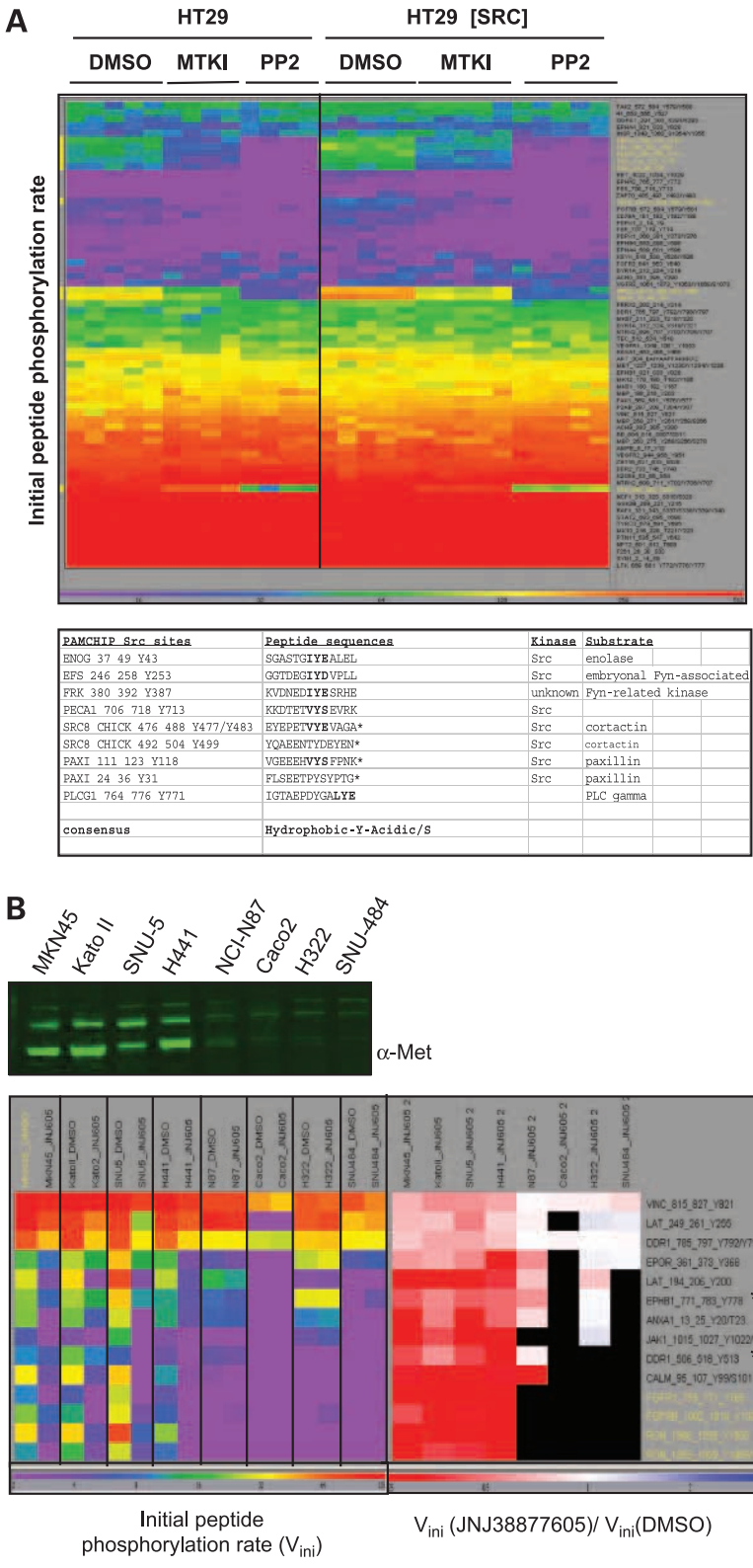

PAMCHIP Src sites	Peptide sequences	Kinase	Substrate
ENOG 37 49 Y43	SGASTG**IYE**ALEL	Src	enolase
EFS 246 258 Y253	GGTDEG**IYD**VPLL	Src	embryonal Fyn-associated
FRK 380 392 Y387	KVDNED**IYE**SRHE	unknown	Fyn-related kinase
PECA1 706 718 Y713	KKDTET**VYS**EVRK	Src	
SRC8 CHICK 476 488 Y477/Y483	EYEPET**VYE**VAGA*	Src	cortactin
SRC8 CHICK 492 504 Y499	YQAEENTYDEYEN*	Src	cortactin
PAXI 111 123 Y118	VGEEEH**VYS**FPNK*	Src	paxillin
PAXI 24 36 Y31	FLSEETPYSYPTG*	Src	paxillin
PLCG1 764 776 Y771	IGTAEPDYGA**LYE**		PLC gamma
consensus	Hydrophobic-Y-Acidic/S		

Figure 2. Src- and MET-selective peptides. **A,** HT29 cells, transfected with empty vector or human Src, were lysed and incubated with DMSO, 5 μmol/L MTKI or PP2, and applied on the peptide arrays. Initial velocity of peptide phosphorylation is represented according to the color legend indicated at the bottom (*purple*, slowest rate of phosphorylation; *red*, fastest rate of phosphorylation). Highlighted peptides are Src selective and are listed in the accompanying table with their peptide sequence. **B,** indicated cell lines with high, intermediate, or low MET levels are analyzed by immunoblot or peptide phosphorylation. Median of six replicate measurements is shown for the initial velocities of peptide phosphorylation in the absence (DMSO) or presence of 1 μmol/L of the MET inhibitor JNJ-38877605 ("605"). *Left,* initial velocity of peptide phosphorylation is represented according to the color legend indicated at the bottom (*purple*, slowest rate of phosphorylation; *red*, fastest rate of phosphorylation); *right,* ratio of the initial velocity in the presence of JNJ-38877605 over the velocity in the absence of compound (DMSO). Legend is depicted at the bottom of the figure: *red,* inhibition of phosphorylation rate by the compound; *white,* no change; *blue,* a stimulation (legend ranges from 4-fold inhibition to 4-fold stimulation). *Black boxes,* undetectable signals in the DMSO condition (and hence no meaningful ratio can be calculated). Phosphorylation of peptides indicated with an asterisk is decreased by the MET inhibitor Su11274 in MKN45 cells as determined by mass spec (25).

cancer cell line NCI-N87) or low/undetectable MET expression (gastric cancer cell line SNU484, NSCLC line H322, and colorectal cancer cell line Caco2; Fig. 2C and Table S1). Phosphorylation of four peptides (peptides highlighted in Fig. 2C) is only detected ($V_{ini} > 4$) in lysates derived from high MET-expressing cell lines, and phosphorylation of

these peptides is completely inhibited by 1 μmol/L JNJ-38877605, arguing that these peptides are selective MET substrate peptides, at least in this panel of eight cell lines. Note that this MET-specific subset contains two peptides derived from the RTK RON, the closest homologue to MET. JNJ-38877605 does not inhibit RON at 1 μmol/L, but these sites in RON are targets for phosphorylation by MET on heterodimerization (23). In addition to these specific MET substrate peptides, phosphorylation of several other peptides correlates well with MET activity in spite of the fact that these peptides are not uniquely phosphorylated by MET (nonhighlighted peptides in Fig. 2C): the partial inhibition of phosphorylation of these peptides by JNJ-38877605 shows that a significant fraction of their phosphorylation is related to MET activity and allows for the detection of low MET activity in NCI-N87 lysates, in addition to the high MET activity in the four MET-overexpressing cell lines. Note that several of these peptides have previously been associated with MET activity: Y20 in Annexin A1 has been reported to be a substrate site of MET (24), and more recently, a mass spec approach uncovered also sites in DDR1 (Y513 as well as Y796 and/or Y797) and a site in EphB4 (Y774), which is analogous to Y778 in EphB1 identified here, as MET-dependent sites (25). Our findings suggest that these sites are indeed direct phosphorylation sites of MET. Hence, profiling lysates on the arrays, particularly in the presence and absence of a kinase inhibitor, represents a useful high-throughput methodology to analyze kinase activities in crude cell lysates.

Identification of Signature Peptides in a 27-Cell Line Panel

We next tested whether the peptide arrays would be a useful tool to predict the response of cell lines to the multitargeted tyrosine kinase inhibitor MTKI. MTKI inhibits the proliferation of a range of cancer cell lines *in vitro* with widely varying IC_{50}s [as determined using 3-(4,5-dimethylthiazol-2-yl)-2,5-diphenyltetrazolium bromide and Alamar blue assays; Fig. 3A]. In this panel, 13 cancer cell lines were defined as "responder" cell lines (IC_{50}, <3 μmol/L), whereas 14 cancer cell lines are defined as "nonresponder" cell lines (IC_{50}, >10 μmol/L). We profiled the lysates, prepared from 27 cell lines, representing diverse tissue types, on the peptide arrays in the presence and absence of 5 μmol/L MTKI, in six replicates for each condition. The data were analyzed as described above. The experiment included the highly responsive H3255 NSCLC cell line, which contains a gene amplification of the mutant EGFR (L858R; Fig. 3B and C, *far left lanes*). EGFR (L858R) is highly responsive to MTKI, which is an ATP-competitive compound that binds to the active conformation of EGFR (similar to erlotinib and gefitinib but unlike lapatinib; Supplementary Table S2; ref. 26). Accordingly, the most profound changes induced by MTKI in lysate kinase activity can be observed for this highly responsive cell line.

The high-content nature of Pamgene peptide array technology allows for the identification of the peptides that serve as the best markers for MTKI response. Hence, we tested for every peptide whether the phosphorylation change by MTKI was significantly different between responding and nonresponding cell lines, taking the interreplicate variability into account (see Materials and Methods for a more detailed description of the statistical test). The

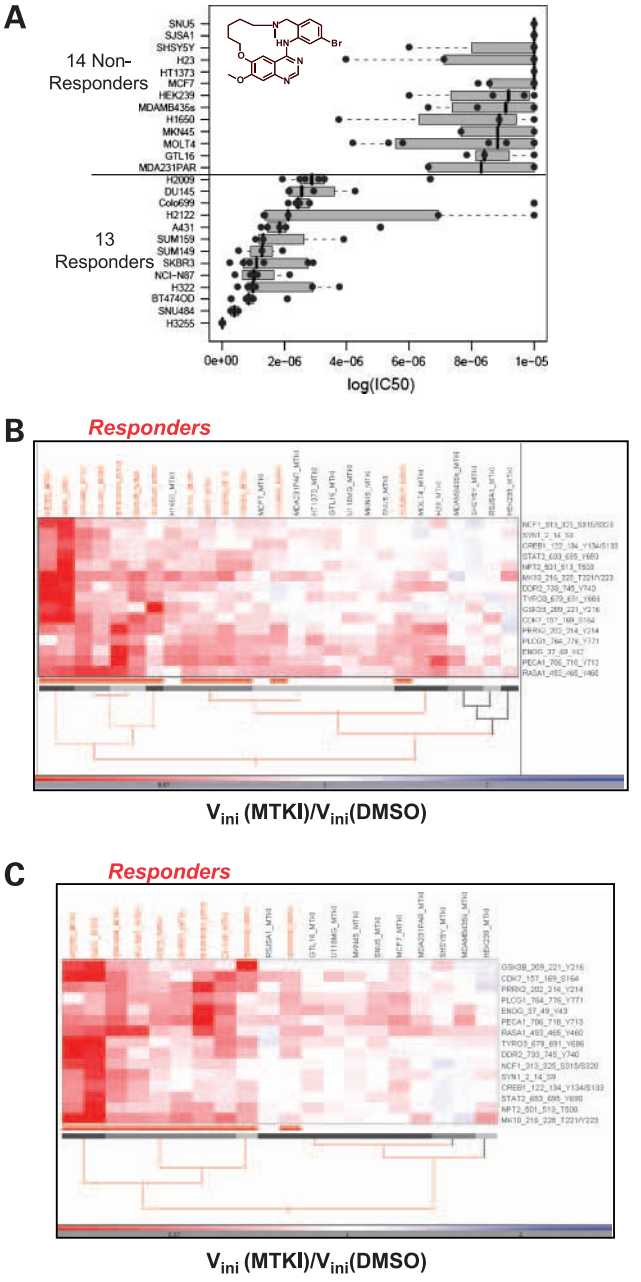

Figure 3. Response prediction to MTKI in cancer cell lines. **A,** inhibition of cell proliferation by MTKI in 27 cell lines. Each dot represents an individually determined IC_{50}. Cell lines are divided in responder and nonresponder cell lines as explained in the text. **B,** profile of MTKI-mediated inhibition of phosphorylation of 16 signature peptides in all 27 cell lines (legend ranges from 2-fold inhibition to 2-fold stimulation). Cell lines were clustered using an unsupervised hierarchical clustering method. *Red,* responder cell lines. **C,** profile of MTKI-mediated inhibition of phosphorylation of 16 signature peptides in 20 cell lines (all mutant RAS and PTEN cell lines have been excluded; see text for details). Cell lines were clustered using an unsupervised hierarchical clustering method. Responder cell lines are highlighted.

top 16 peptide phosphorylations that were significantly changed by MTKI treatment with a false discovery rate of less than 10% were invariably inhibitions (see Supplementary Table S3). The inhibition of phosphorylation by MTKI of the signature peptide set in the 27 cell lines is illustrated in Fig. 3B, where the cell lines have been clustered in an unsupervised manner according to the behavior of the 16 signature peptides (responder cell lines are highlighted in columns, and Src-selective peptides are highlighted in rows). The result is a clear responder cluster containing 7 responders, a nonresponder cluster containing 4 nonresponders, and a mixed cluster of 6 responders and 10 nonresponders. The mixed group contains many cell lines with activating mutations in RAS, and deletion in PTEN, both resulting in constitutive (i.e., RTK independent) signaling (and proliferation and survival). Those mutations will confer resistance to MTKI regardless of the (over) expression of its target tyrosine kinases and, hence, might interfere in correctly classifying nonresponder cell lines based on the inhibition of protein tyrosine kinase activity in the lysates. We therefore repeated the cell line clustering in the absence of those cell lines containing activating RAS mutations (H1373, H2009, Colo699, H23, H2122, and MOLT4; all cell lines have been profiled for K-RAS status in house) and PTEN inactivation (MOLT4 and H1650, both verified in house; note that H1650 contains also a small internal deletion in exon 19 of EGFR that renders the RTK sensitive to MTKI inhibition). Of the remaining 20 cell lines (10 responders and 10 nonresponders), all but one (the responder, SUM159) are correctly classified using the same unsupervised clustering algorithm used above (see Fig. 3C).

Statistical Analysis of Response Prediction Accuracy

To test the predictive value of the signature peptides, we applied different classification algorithms to the data set introduced in the previous paragraph. Training and test cell lines were independent during the classification exercise (see Materials and Methods for more details). As expected from the literature (27), Random Forest was the best performing classifier, although Support Vector Machine and Bagging performed almost equally well. The overall response prediction of the 27-cell line panel was moderately accurate, with average misclassification rates of 25% with Random Forest. For most classification algorithms, misclassification error decreased by increasing

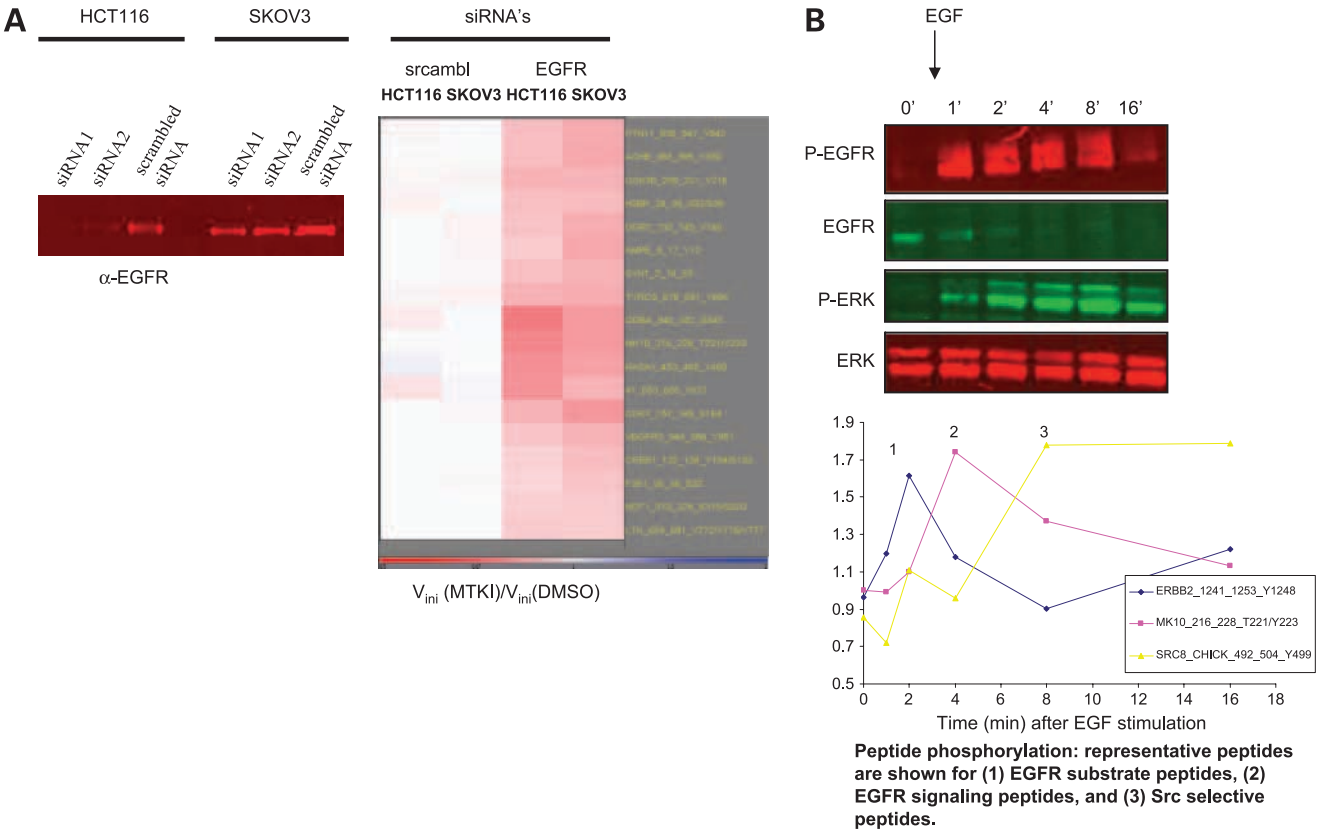

Figure 4. Characterization of EGFR-sensitive peptides. **A,** HCT116 and SKOV-3 cells were transfected with siRNAs against EGFR or a scrambled control. The ratio shown is the initial velocity in the EGFR siRNA-transfected cells (in six replicates) over the velocity in the cells transfected with a scrambled control. **B,** EGF stimulation of HeLa cells. Lysates were analyzed by immunoblot (*top*; quantification on the right) or peptide phosphorylation (*bottom*; ratio of median phosphorylation of four replicates after EGF stimulation over phosphorylation before addition of EGF). Three exemplary peptides are shown, and more peptides are listed in Supplementary Table S5.

Table 1. Effect of MTKI on eight xenograft tumors (treatment/control ratios)

Cell line	Type	Drug dose (mg/kg)	Formulation	Duration (d)	Route	Schedule	T/C value
NCI-H3255	NSCLC	125	30% (w/v) SBE-β-CD	28	P.o.	bd	–79.5%
A431	Skin epidermoid carcinoma	75	30% (w/v) SBE-β-CD	34	P.o.	qd	10.4%
NCI-H322	Bronchioalveolar NSCLC	125	30% (w/v) SBE-β-CD	28	P.o.	bd	–5.9%
DU145	Prostate carcinoma	125	30% (w/v) SBE-β-CD	28	P.o.	bd	23.6%
NCI-H1703	Squamous cell, adenocarcinoma; NSCLC	125	30% (w/v) SBE-β-CD	42	P.o.	bd	85.8%
SKOV-3	Ovarian adenocarcinoma	100	20% (w/v) HP-β-CD	17	P.o.	qd	72.4%
NCI-H460	Carcinoma; large cell lung cancer	125	30% (w/v) SBE-β-CD	19	P.o.	bd	117.0%
HT29	Colorectal adenocarcinoma	200	30% (w/v) SBE-β-CD	28	P.o.	qd	63.7%

Abbreviations: SBE-β-CD, sulfobutyl ether β-cyclodextrin (Captisol); HP-β-CD, hydroxypropyl-β-cyclodextrin; bd, twice daily; qd, once daily; T/C, treatment/control (T/C) ratios were calculated based on the change in final median or relative tumor volumes using the National Cancer Institute criteria—"The effective criteria for T/C ratios is 42%" (32).

the signature size from two to seven peptides. Using more than seven peptides did not improve classification accuracy considerably (data not shown). Of the 7 most frequently selected peptides in the classification models, 4 were in the 16-peptide signature set derived on the entire data set using the mixed model described in the previous paragraph (Supplementary Table S4). The overall misclassification rate of 25% was primarily caused by eight cell lines that were often misclassified (Supplementary Fig. S3). Consistent with the unsupervised clustering results, six of the eight misclassified cell lines were either RAS mutant or PTEN negative (Fig. 3C; Supplementary Fig. S3). The classification accuracy improved considerably when only including RAS and PTEN wild-type cell lines: the average misclassification rate dropped to 8.7% with an optimal number of peptides between 3 and 5. All cell lines were in general correctly classified (Supplementary Fig. S4), except cell line SUM149, which was only 51.5% of the times correctly classified. The five most frequently selected peptides (Supplementary Table S4) strongly overlap with the signature peptides derived before (four of five). In summary, response prediction to MTKI is highly accurate (91%) after exclusion of RAS mutants and PTEN-negative cell lines.

Biological Validation of the Cell Line–Derived Phosphopeptide Signature

Three of 16 signature peptides for MTKI are Src-selective substrates (compare Figs. 2A and 3C; peptides in ENOG, PLCG1, and PECA1), indicating that inhibition of Src activity by MTKI contributes to the *in vitro* efficacy of the compound in this 27-cell line panel. To determine which other kinases are involved in the antiproliferative effect of MTKI, we first compared the effect of siRNA knockdown of the major target of MTKI (i.e., EGFR) in two cell lines (HCT116 and SKOV-3). The analysis of this siRNA experiment is shown in Fig. 4A, where all 18 peptides that are significantly ($P < 0.05$) reduced by siRNA against EGFR, but not a control scrambled siRNA or siRNAs against Src (cfr. Fig. 2), in both cell lines are shown. Importantly, more than half of the peptides in the MTKI signature set (9 of 16) are also affected by the siRNA against EGFR (compare Figs. 3B and 4A), indicating that the majority of the peptides that determine sensitivity toward MTKI in a cell proliferation experiment are related to EGFR signaling. A notable example of such overlapping peptides is a peptide containing Y460 in RASGAP (RASA1), which is a well-established phosphorylation site of EGFR *in vitro* and in cells (28). To test which of those EGFR-responsive peptides are direct EGFR substrates, we stimulated HeLa and H322 cells with EGF and harvested samples after 1, 2, 4, 8, and 16 minutes. As illustrated in Fig. 4B and Supplementary Table S5, several peptides increased immediately (i.e., at 1 minute) after EGF stimulation and returned to their basal level after 4 to 8 minutes; the phosphorylation kinetics of those peptides mimic EGFR autophosphorylation (Fig. 4B, *top*), and hence, these peptides likely represent direct EGFR substrates. As expected, the MTKI cell line signature peptide set contains many direct EGFR substrate peptides (6 of 16). On the other hand, several peptides increased only after 4 minutes of EGF stimulation or even later; these peptides are likely targets of kinases that are activated downstream of EGFR activation. One clear-cut example of the latter is the activation of Src kinase activity, as shown by the coordinate upregulation of the phosphorylation rate of the Src-selective peptides. In HeLa cells, activation of this peptide subset occurred only 8 to 16 minutes after EGF stimulation (Fig. 4B, *bottom*), in accordance with the purported phosphorylation of several Src targets with those kinetics after EGF stimulation of HeLa cells, determined by mass spectrometry (29).[6] The identity of some of the other peptides that are phosphorylated 4 to 8 minutes after EGF stimulation is suggestive: for instance, an increase of the phosphorylation of a peptide derived from mitogen-activated protein kinase (MK10_216_228_T221/Y223) may reflect activation of mitogen-activated protein kinase signaling. Interestingly, the MTKI cell line signature peptide set contains also two such EGFR signaling peptides that are not Src selective (Supplementary Table S5), suggesting that not only direct EGFR and Src inhibition by MTKI is important for the response classification but also the—possibly indirect—inhibition of

[6] http://www.phosida.org

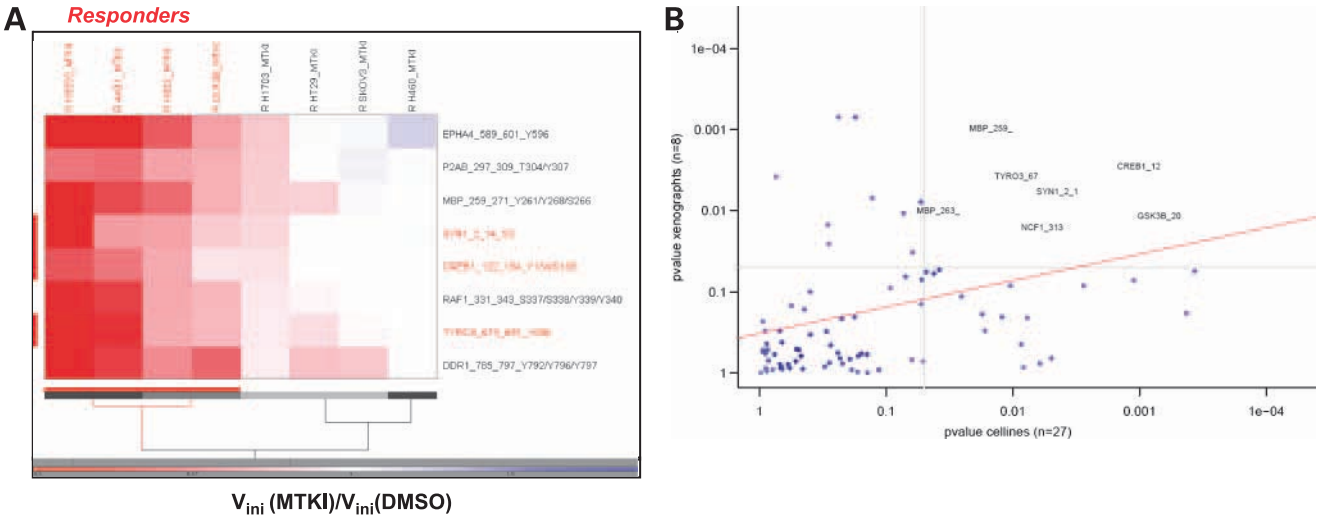

Figure 5. MTKI response prediction in xenograft tumors. **A,** profile of MTKI (5 μmol/L)–mediated inhibition of phosphorylation of signature peptides in eight xenograft tumor lysates. Peptide phosphorylation analysis on the 144-peptide array. Legend is indicated at the bottom of each figure (range between 2-fold inhibition and 2-fold stimulation of peptide phosphorylation by MTKI). **B,** correlation between likelihood (uncorrected *P* values) of interaction between peptide phosphorylation inhibition by MTKI and response status to MTKI in cell lines and xenograft tumors.

other kinases downstream of EGFR. Finally, there is a large overlap between EGFR substrate and signaling peptides (identified in EGF-stimulated H322 and HeLa cells) on the one hand and peptides whose phosphorylation is inhibited by EGFR siRNA in HCT116 and SKOV-3 cells on the other hand (compare Fig. 4A and Supplementary Table S5: 11 peptides in common). The peptide inhibition pattern of siRNA against Her2 (in BT474 breast cancer cells) largely overlapped with those peptides found for EGFR siRNA (data not shown; cfr. Fig. 4A). In summary, these findings argue for EGFR/Her family inhibition as the primary reason for inhibition of cell proliferation by MTKI in this cell line panel but indicate that inhibition of Src activity also has a role toward the *in vitro* activity of this compound in a significant subset of these 27 cell lines.

Identification of Signature Peptides in Xenograft Tumors

To explore whether a similar approach allows for the classification of responder and nonresponder tumors, we applied the same strategy as above to eight different xenograft tumors, which were s.c. grown in nude immunocompromised mice from human cancer cell lines. These tumors can be divided in four MTKI-responsive tumors and four nonresponsive tumors. The responsive tumors are arranged according to their responsiveness to MTKI in mice, ranging from tumor regression of H3255 and H322 xenograft tumors, potent tumor growth inhibition of A431, to significant inhibition of tumor growth for DU145 (prostate; Table 1; ref. 21). The nonresponsive tumors [H460 and H1703 (lung), SKOV-3 (ovarian), and HT29 (colon)] are all nonresponsive to MTKI *in vivo* according to the National Cancer Institute criteria (see Table 1). Lysates were made from homogenized frozen tumor blocks (see Materials and Methods) and analyzed in the presence or absence of 5 μmol/L MTKI, as before. Overall, the phosphorylation rate of most peptides was significantly faster in tumor lysates compared with the corresponding cell lines (data not shown). A statistical test was applied to this data set, similar as before for the 27 cell lines, and the 8 peptides that discriminate between responders and nonresponders with a false discovery rate of <10% are shown in Supplementary Table S6. Unsupervised hierarchical clustering of these data separated all four responder tumors from all four nonresponder tumors (Fig. 5A). Notably, a good correlation between the degree of tumor response and the degree of inhibition of peptide phosphorylation by MTKI in tumor lysates was observed (compare Fig. 5A with Table 1). Three of the peptides in this tumor signature set were also found in the cell line signature set, indicating that inhibition of some of the same kinases is critical to reduce tumor growth compared with inhibition of growth *in vitro* but also pointing to the importance of other kinases in the *in vivo* setting. Although three "EGFR substrate peptides" and one "EGFR signaling peptide" are present in the eight-peptide MTKI tumor signature, no Src-specific peptides are represented, suggesting that Src inhibition by MTKI, in contrast to EGFR inhibition, does not contribute to the response of these eight xenograft tumors. Comparing inhibition of peptide phosphorylation by MTKI in 27 cell line lysates and 8 xenograft tumor lysates results in a statistically significant correlation between the two data sets when considering all peptides ($P < 0.0001$, Spearman rank correlation; Fig. 5B). More importantly, a subset of peptides serves as indicators of response to MTKI in both cell and tumor lysates (peptides in the *top right corner* of Fig. 5B).

Discussion

The major intrinsic drawback of using peptide arrays to deconvolute kinase activities in a complex mixture, such as

crude cell lysates, is the limited specificity associated with *in vitro* phosphorylation of peptides. Primary sequence context only explains ~25% of the enzyme-substrate specificity seen in cells, with the remainder of the specificity determined through kinase-substrate coexpression or subcellular colocalization, and protein docking or scaffolding (30). Hence, for the majority of kinases, it is difficult to find a single peptide substrate that is specific to a single kinase in the presence of hundreds of other active kinases. In the present study, we found that three parameters can greatly improve the utility of peptide phosphorylation in lysates: (*a*) the use of kinetic phosphorylation rates rather than end point measurements, (*b*) the use of coordinately phosphorylated peptide sets rather than relying on individual peptides, and, most importantly, (*c*) the use of compound-mediated inhibition of peptide phosphorylation rates. We have shown for three distinct tyrosine kinases (Src, EGFR, and MET) that specific peptide sets can be found to correlate with their respective kinase activities in cell lysates. In the case of Src and MET, many of these peptides were derived from known or presumed *in vivo* substrate sites. In the case of EGFR (and Her2), no such clear relation to known substrates was found in most cases, and phosphorylation of the identified EGFR substrates was only modestly inhibited by a potent EGFR inhibitor and, similarly, was only modestly induced by EGF stimulation. Nevertheless, even those "moderately specific" peptides proved valuable in classifying responder and nonresponder cells based on the inhibition of peptide phosphorylation by MTKI in 27 cell lines or 8 xenograft tumors. An attractive possibility to improve the value of the standard 144-peptide array is to expand the peptide set with more "kinase-selective" peptides. The knowledge of phosphopeptide sites is rapidly growing due to several large-scale phosphopeptide mass spectrometry efforts.[7] These public databases provide an excellent starting point for the improvement of the tyrosine peptide content of the current arrays.

The cell line classification experiment pointed out a limitation of the response prediction methodology: when response to a compound is determined by mechanisms downstream, and independent of, the target kinase(s), the method largely fails. RTK-independent signaling by RAS mutants or loss of PTEN was not accurately predicted. Hence, application of this method should be directed to cases where response is largely determined by the activity (i.e., expression level and/or mutational status) of the target kinases themselves. In the case of EGFR inhibitors, genetic testing for RAS mutants or PTEN status can be used as exclusion criteria. For other tyrosine kinases, such as ABL, PDGFR, and KIT, resistance has mostly been attributed to mutations in the protein tyrosine kinases. Indeed, lysates from Ba/F3 cells expressing BCR-ABL mutants with varying sensitivity to imatinib can be accurately classified based on the imatinib-mediated inhibition of phosphorylation of a subset of "imatinib signature peptides" (31).[8] This response prediction methodology allows to define a specific signature peptide sets for, in principle, any tyrosine kinase inhibitor, regardless of the breadth of its target spectrum and irrespective of the knowledge of the relevant targets. Provided that nonfixed (frozen) biopsies of a tumor are available, kinase detection in lysates from these biopsies (5–10 μg of protein extract or a 10- to 20-μm cryosection is sufficient per peptide array), in the presence and absence of a range of kinase inhibitors, should allow the ideal match between a given tumor tyrosine kinase profile and a compound inhibition spectrum. Another critical aspect of response prediction tools is their sensitivity to sample heterogeneity. We have tested this aspect by diluting xenograft tumor lysates with normal lung tissue lysate. Kinase activity of the latter was relatively high compared with the xenograft tumor material, yet the peptide phosphorylation inhibition signature (i.e., the ratio of phosphorylation in the presence of DMSO over the phosphorylation in the presence of compound) identified the mixed lysates as responsive to the compound (MTKI or JNJ-38877605) down to a 50% dilution of the tumor lysates with the normal tissue lysate—the most specific peptides being the most robust indicators of response (data not shown).

In addition to the response prediction application of the technology highlighted here, multiwell peptide arrays with a kinetic readout are also useful to compare kinase inhibition signatures for several multitargeted kinase inhibitors in cell and tumor lysates. These compound signatures enable selection of kinase inhibitors and define the critical target(s), if a peptide set, of which the inhibition of phosphorylation correlates to response, can be unambiguously linked to a kinase of interest. The latter should enable mode-of-action studies of multitargeted tyrosine kinase inhibitors in xenograft tumor models. Finally, the method can be exploited as a pharmacodynamic readout of inhibition of multiple kinases and, as such, be used in dose-finding studies.

Disclosure of Potential Conflicts of Interest

All authors are employees of Ortho Biotech Research and Development, a division of Janssen Pharmaceutical. M. Versele, T. Perera, and W. Talloen: coinventors on a patent relating to this article. No other potential conflicts of interest were disclosed.

Acknowledgments

We thank all people at Pamgene (Den Bosch, the Netherlands) for their technical support during this work and many colleagues at Janssen Pharmaceutica for their critical feedback during the course of this study and on the manuscript.

References

1. Ohno R. Treatment of chronic myeloid leukemia with imatinib mesylate. Int J Clin Oncol 2006;11:176–83.

2. Sciot R, Debiec-Rychter M. GIST under imatinib therapy. Semin Diagn Pathol 2006;23:84–90.

3. Lasota J, Miettinen M. KIT and PDGFRA mutations in gastrointestinal stromal tumors (GISTs). Semin Diagn Pathol 2006;23:91–102.

4. Tamborini E, Bonadiman L, Greco A, et al. A new mutation in the KIT ATP pocket causes acquired resistance to imatinib in a gastrointestinal stromal tumor patient. Gastroenterology 2004;127:294–9.

[7] See for example: www.phosida.org and www.phosphosite.org.
[8] M. Versele and J. Cools, unpublished results.

5. Branford S, Rudzki Z, Walsh S, et al. High frequency of point mutations clustered within the adenosine triphosphate-binding region of BCR/ABL in patients with chronic myeloid leukemia or Ph-positive acute lymphoblastic leukemia who develop imatinib (STI571) resistance. Blood 2002;99: 3472–5.

6. Kris MG, Natale RB, Herbst RS, et al. Efficacy of gefitinib, an inhibitor of the epidermal growth factor receptor tyrosine kinase, in symptomatic patients with non-small cell lung cancer: a randomized trial. JAMA 2003; 290:2149–58.

7. Paez JG, Janne PA, Lee JC, et al. EGFR mutations in lung cancer: correlation with clinical response to gefitinib therapy. Science 2004;304: 1497–500.

8. Lynch TJ, Bell DW, Sordella R, et al. Activating mutations in the epidermal growth factor receptor underlying responsiveness of non-small-cell lung cancer to gefitinib. N Engl J Med 2004;350:2129–39.

9. Takano T, Ohe Y, Sakamoto H, et al. Epidermal growth factor receptor gene mutations and increased copy numbers predict gefitinib sensitivity in patients with recurrent non-small-cell lung cancer. J Clin Oncol 2005;23: 6829–37.

10. Cho BC, Im CK, Park MS, et al. Phase II study of erlotinib in advanced non-small-cell lung cancer after failure of gefitinib. J Clin Oncol 2007;25: 2528–33.

11. Pao W, Miller VA, Politi KA, et al. Acquired resistance of lung adenocarcinomas to gefitinib or erlotinib is associated with a second mutation in the EGFR kinase domain. PLoS Med 2005;2:e73.

12. Engelman JA, Mukohara T, Zejnullahu K, et al. Allelic dilution obscures detection of a biologically significant resistance mutation in EGFR-amplified lung cancer. J Clin Invest 2006;116:2695–706.

13. Massarelli E, Varella-Garcia M, Tang X, et al. KRAS mutation is an important predictor of resistance to therapy with epidermal growth factor receptor tyrosine kinase inhibitors in non-small-cell lung cancer. Clin Cancer Res 2007;13:2890–6.

14. Buckingham LE, Coon JS, Morrison LE, et al. The prognostic value of chromosome 7 polysomy in non-small cell lung cancer patients treated with gefitinib. J Thorac Oncol 2007;2:414–22.

15. Bantscheff M, Eberhard D, Abraham Y, et al. Quantitative chemical proteomics reveals mechanisms of action of clinical ABL kinase inhibitors. Nat Biotechnol 2007;25:1035–44.

16. Frank O, Brors B, Fabarius A, et al. Gene expression signature of primary imatinib-resistant chronic myeloid leukemia patients. Leukemia 2006;20:1400–7.

17. Balko JM, Potti A, Saunders C, Stromberg A, Haura EB, Black EP. Gene expression patterns that predict sensitivity to epidermal growth factor receptor tyrosine kinase inhibitors in lung cancer cell lines and human lung tumors. BMC Genomics 2006;7:289.

18. Huang F, Reeves K, Han X, et al. Identification of candidate molecular markers predicting sensitivity in solid tumors to dasatinib: rationale for patient selection. Cancer Res 2007;67:2226–38.

19. Lemeer S, Ruijtenbeek R, Pinkse MW, et al. Endogenous phosphotyrosine signaling in zebrafish embryos. Mol Cell Proteomics 2007;6: 2088–99.

20. Bain J, Plater L, Elliott M, et al. The selectivity of protein kinase inhibitors: a further update. Biochem J 2007;408:297–315.

21. Perera T, Versele M, Lavrijssen T, et al. JNJ-26483327 is a novel multi-targeted tyrosine kinase inhibitor with cellular activity against EGFR, Her2, Src and VEGFR3. EJC 2006;Suppl 4:178.

22. Perera T, Lavrijssen T, Janssens B, et al. JNJ-38877605: a selective Met kinase inhibitor inducing regression of Met-driven tumor models [abstract 4837]. AACR Meeting Abstracts 2008:4837.

23. Follenzi A, Bakovic S, Gual P, Stella MC, Longati P, Comoglio PM. Cross-talk between the proto-oncogenes Met and Ron. Oncogene 2000; 19:3041–9.

24. Skouteris GG, Schröder CH. The hepatocyte growth factor receptor kinase-mediated phosphorylation of lipocortin-1 transduces the proliferating signal of the hepatocyte growth factor. J Biol Chem 1996;271: 27266–73.

25. Guo A, Villén J, Kornhauser J, et al. Signaling networks assembled by oncogenic EGFR and c-Met. Proc Natl Acad Sci U S A 2008;105:692–7.

26. Wood ER, Truesdale AT, McDonald OB, et al. A unique structure for epidermal growth factor receptor bound to GW572016 (lapatinib): relationships among protein conformation, inhibitor off-rate, and receptor activity in tumor cells. Cancer Res 2004;64:6652–9.

27. Lee JW, Lee JB, Park M, Song SH. An extensive comparison of recent classification tools applied to microarray data. Comput Stat Data Anal 2005;48:869–85.

28. Liu XQ, Pawson T. The epidermal growth factor receptor phosphorylates GTPase-activating protein (GAP) at Tyr-460, adjacent to the GAP SH2 domains. Mol Cell Biol 1991;11:2511–6.

29. Olsen JV, Blagoev B, Gnad F, et al. Global, *in vivo*, and site-specific phosphorylation dynamics in signaling networks. Cell 2006;127:635–48.

30. Linding R, Jensen LJ, Ostheimer GJ, et al. Systematic discovery of *in vivo* phosphorylation networks. Cell 2007;29:129:1415–26.

31. De Keersmaecker K, Versele M, Cools J, Superti-Furga G, Hantschel O. Intrinsic differences between the catalytic properties of the oncogenic NUP214-ABL1 and BCR-ABL1 fusion protein kinases. Leukemia 2008;22: 2208–16.

32. Bissery M-C, Chabot GG. History and new development of screening and evaluation methods of anticancer drugs used *in vivo* and *in vitro*. Bull Cancer 1991;78:587–602.